MODELING INTERPLANETARY DUST DISTRIBUTION

J.-J. Wasbauer[1], M. Blanc[1], F. Alby[2], P. Chèoux-Damas[3]

[1] Observatoire Midi-Pyrénées, 14 avenue E. Belin, 31400 Toulouse, France
[2] Centre National d'études Spatiales, 18 avenue E. Belin, 31401 Toulouse cedex 4, France
[3] Matra Marconi Space, 31 rue des cosmonautes, 31402 Toulouse cedex 4, France

ABSTRACT

Dust particles orbit the Sun with velocities of tens of km/s and represent hazard for space vehicles. They also carry some information about the solar system structure and its evolution. Knowing more about them increases our knowledge about the behavior of the interplanetary medium.
This paper presents the mathematical expansions set up to take the impacting directionality in both the $(m, r_0, v_{0r}, v_{0t}, v_{0z})$ and the keplerian invariants phase space into account. We assume axisymmetry of the cloud and symmetry about the ecliptic plane. A bi-gaussian model with both in-ecliptic and out-of-ecliptic temperatures is worked out thanks to an algorithm which minimizes the error in fitting the full set of available data. It fits the flux along Galileo trajectory but needs at least the interstellar contribution to fit the flux detected on-board Ulysses.
This formalism produces an analytical out-of-ecliptic mapping of the velocity distribution and allows to compute macroscopic quantities. The adiabatic invariant description opens possibilities for a secular evolution model.

1. INTRODUCTION

Ulysses and Galileo have enriched our knowledge of interplanetary dust populations with directional information. Adding these new observations to the previous ones, we defined a new a priori mathematical representation of the cloud. It finds its root in the equivalence between in-ecliptic description and adiabatic invariants phase space. Hyperbolic and elliptic trajectories are treated in the same way. The available data is sorted in a database which may be updated with future data of upcoming missions.
We will first introduce the canonical variables in the invariant phase space and the main symmetry assumptions made to reduce the number of descriptive variables. Then we produce the new parametric mathematical representation from the in-ecliptic distribution function and its attached statistics. The model parameters are tuned to minimize the error made while reproducing the measurements. Finally the resulting model is compared to Galileo and Ulysses data to evaluate its quality.

2. MATHEMATICAL REPRESENTATION OF THE DUST POPULATION

The dust cloud has a complex behavior. Each particle is submitted to several physical processes. The main force is Sun gravity but the keplerian motion is perturbed by secondary dissipative effects which structure the mass and velocity distributions. For small particles the Poynting-Robertson effect competes with radiation pressure whose apparent effect is to reduce the solar attraction. The former one spirals the particles towards the Sun whereas the latter may drive particles on hyperbolic motion after fragmentation or collision in the vicinity of the Sun where the density is higher. For very small particles, electromagnetic field enhances the dispersion of the velocity. In this study we will not try to reproduce these effects but we will present an a-priori mathematical representation of the dust population, assuming that on a short time scale the orbit of each particle is keplerian.

2.1 Adiabatic invariants of the keplerian motion

In the action-angle set of variables defined in classical mechanics actions are adiabatic invariants. For cyclic motions such as keplerian closed orbits, they can be derived using the orbital parameters (a, e, i, w, Ω, M)

$$\begin{aligned} \mathcal{L} &= \sqrt{\mu a}, & l &= M = n(t - t_0), \\ \mathcal{G} &= \sqrt{\mu a(1-e^2)}, & g &= w, \\ \mathcal{H} &= \sqrt{\mu a(1-e^2)}\cos i, & h &= \Omega. \end{aligned} \qquad (1)$$

The set $(\mathcal{L}, \mathcal{G}, \mathcal{H}, l, g, h)$ is called the Delaunay variables. $\mathcal{L}$ is directly linked to the total energy $\mathcal{E}$, $\mathcal{G}$ is the magnitude of the angular momentum and $\mathcal{H}$ is the z-component of the angular momentum. Unfortunately the hyperbolic motion is not cyclic, but we know that hyperbolic motions have the same physical origin as the elliptic ones. This origin is gravity. It gives reasons to build an extension of the Delaunay variables for hyperbolic trajectory. l, g, h are kept but $\mathcal{L}, \mathcal{G}, \mathcal{H}$ are extended to

$$\mathcal{L} = -\sqrt{\mu a}, \mathcal{G} = \sqrt{\mu a(e^2-1)}, \mathcal{H} = \sqrt{\mu a(e^2-1)}\cos i \qquad (2)$$

The Jacobean function of the transformation from position-momentum space to this new set of variables is equal to 1. This shows its canonicity.

2.2 Choice of variables

The whole $(\mathcal{L}, \mathcal{G}, \mathcal{H})$ space is not accessible. Both couples $(\mathcal{L}, \mathcal{G})$ and $(\mathcal{G}, \mathcal{H})$ must verify the following inequalities

$$\frac{\mathcal{G}}{\mathcal{L}} = \sqrt{1-e^2} \le 1 \text{ and } |\mathcal{H}| \le \mathcal{G}, \qquad (3)$$

which define accessible and forbidden zones. The accessible $(\mathcal{L}, \mathcal{G})$ domain is not continuous and we prefer to replace $\mathcal{L}$ by $\mathcal{E}$, where the $(\mathcal{E}, \mathcal{G})$ definition domain is

$$1+\frac{2\mathcal{E}\mathcal{G}^2}{\mu^2}\geq 0. \quad (4)$$

Unfortunately, $(\mathcal{E},\mathcal{G},\mathcal{H},l,g,h)$ is not a canonical set anymore, but the Jacobean function of the transformation is very simple.

2.3 Axisymmetry, symmetry about the ecliptic

Dust cloud observations do not show any strong deviation from axisymmetry about the South-North ecliptic axis. Moreover zodiacal light observations[13] have shown that a plane of symmetry exists very close to the ecliptic (about 7 deg. inclined on the ecliptic plane). As an approximation we will suppose the cloud *axisymmetric* ($\mathbf{H_1}$) and *symmetric about the ecliptic plane* ($\mathbf{H_2}$).

2.4 Relation with the canonical representation

Assumptions $\mathbf{H_1}$ and $\mathbf{H_2}$ involve simplifications in the number of variables used to describe the cloud either in $(r,\theta,z,\mathbf{v})$ or $(\mathcal{E},\mathcal{G},\mathcal{H},M,\omega,\Omega)$ variables. $\mathbf{H_1}$ and $\mathbf{H_2}$ allow us not to consider the azimuthal angle θ and negative z in the classical phase space, and the ascending node Ω in the invariant one. Averaging the number of particles on a single trajectory, we suppress the mean anomaly reducing the descriptive variables to $(\mathcal{E},\mathcal{G},\mathcal{H},\omega)$.

This averaging procedure has consequences on the now reduced (r,z>0,**v**) phase space. We assume that the local particle density on a single trajectory is proportional to the inverse of the velocity magnitude ($\mathbf{H_3}$). Thanks to $\mathbf{H_3}$, we can rebuild the entire distribution along the orbit knowing the number of particles present at one orbital position. The most interesting representing position of the whole trajectory is the ascending node $(r_0,\mathbf{v}_0)$ because every kind of keplerian trajectory has at least one point in the ecliptic. In the particular case of a unique in-ecliptic descending position, $\mathbf{H_1}$ allows us to consider it as the symmetric of an ascending node.

Let f be the velocity distribution in the reduced phase space. The two sets of variables are linked by the following relation

$$f\left(r_0,\vec{\mathbf{v}}_0\right)dr_0\,d\vec{\mathbf{v}}_0=\frac{f\left(\mathcal{E},\mathcal{G},\mathcal{H},\omega\right)}{Q\left(\mathcal{E},\mathcal{G}\right)}\frac{\sqrt{2|\mathcal{E}|}}{\left|\vec{\mathbf{v}}_0\right|}d\mathcal{E}d\mathcal{G}d\mathcal{H}d\omega, \quad (5)$$

where Q is yielded from the normalization of the previously explained spreading model (**H3**) and involves elliptic integrals. The transformation from $(r_0,\mathbf{v}_0)$ to $(\mathcal{E},\mathcal{G},\mathcal{H},\omega)$ is unique.

3. DESCRIPTION AND REDUCTION OF THE DATA

3.1 List of available data, sources

We used two kinds of measurements: in-situ records made on-board space probes, and Earth-bound remote measurements. The most recent in situ data set has been gathered by Grün et al.[4,5] from Galileo and Ulysses dust detectors records. Pioneer[10] 10&11, Helios[11] I and II fluxes and zodiacal light measurements detected along the trajectory are older sources of data.

Earth-bound observations of meteors produced a database of recorded events containing radiant direction and mass estimations which is maintained by IAU[14]. Levasseur-Regourd[13] gathered zodiacal light intensities observed from Earth giving some out-of-ecliptic information. Grün's interplanetary flux[7] gives the dust particles mass distribution at 1AU.

We built a database which contains the necessary information associated to the measurement such as trajectory, sensor detection, detection threshold curve for impact records, or direction of the line of sight and distance of observation for zodiacal light. This database is easy to maintain and may be updated with upcoming measurements from future missions.

3.2 Making use of the Galileo and Ulysses data sets

For each recorded event on-board of Ulysses and Galileo, the detector axis direction, the impact velocity and the impact date have been stored. We removed from the data set[4,5] the following events: events with a too high error factor, events without associated directional information, events within a planet influence sphere, events which are clearly identified to be of interstellar origin.

First, knowing the spacecraft trajectory we computed a raw velocity distribution without taking into account the measurement error. An example of the resulting distribution is shown on Fig.1.

Then we use a Monte-Carlo sampling method to reproduce the measurement error in mass, impact velocity magnitude and impacting direction, using the attached error factors and the relative sensitive area. The uncertainty on the impacting direction smoothes the non significant peaks but keeps the main one (Fig.1).

3.3 Choice of the representation

The distributions in each direction show a strong peak (Fig.1) and decrease very fast for high velocities. Moreover, the physical phenomenon that disperses particles out-of-ecliptic and the one that structures the cloud within the ecliptic are different. For these reasons we represent the cloud by a bi-gaussian function f that includes the mass distribution[7]. The expression is the following

$$f\left(m,r_0,\vec{\mathbf{v}}_{0e},v_{0z}\right)=\frac{h(m)e^{-\left(\frac{v_{0z}-U_z}{\sigma_z\sqrt{2}}\right)^2}e^{-\left(\frac{\vec{\mathbf{v}}_{0e}-\vec{\mathbf{U}}_e}{\sigma_e\sqrt{2}}\right)^2}}{\sigma_e^2\sigma_z\left(\sqrt{2\pi}\right)^3 r_0^{\nu}}, \quad (6)$$

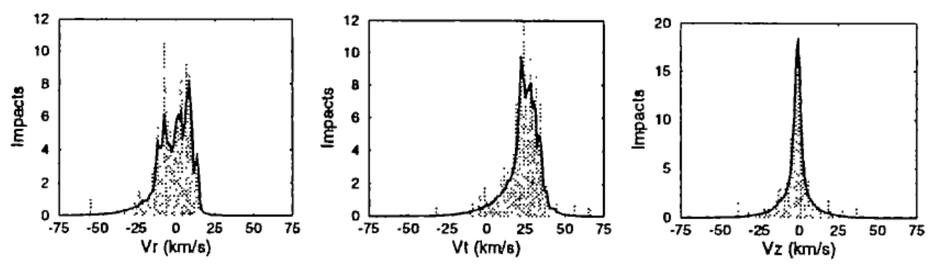

Fig. 1 Velocity distribution. Galileo events at 1.175 AU. Solid line is the Monte-Carlo processed velocity distribution and the shaded distribution is the raw data distribution.

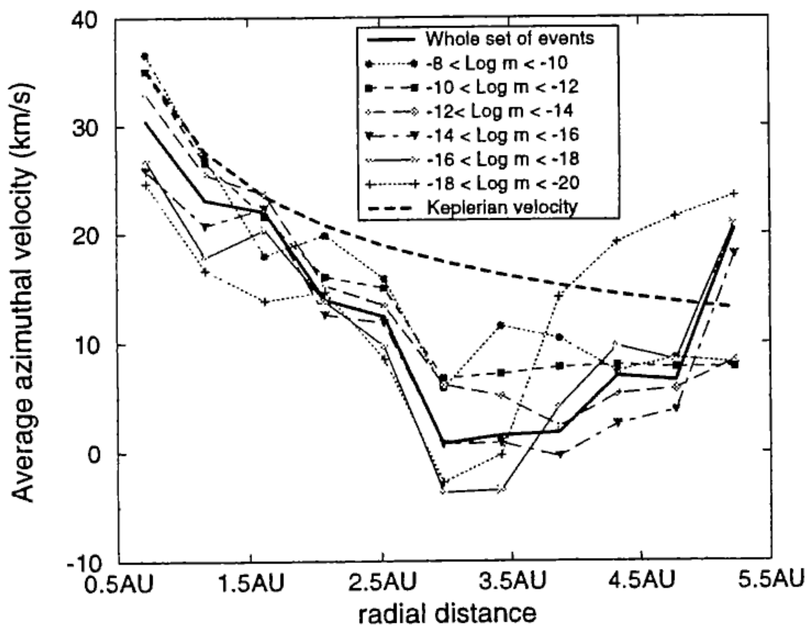

Fig. 2 Average azimuthal velocity as a function of radial distance r_0 and mass m.

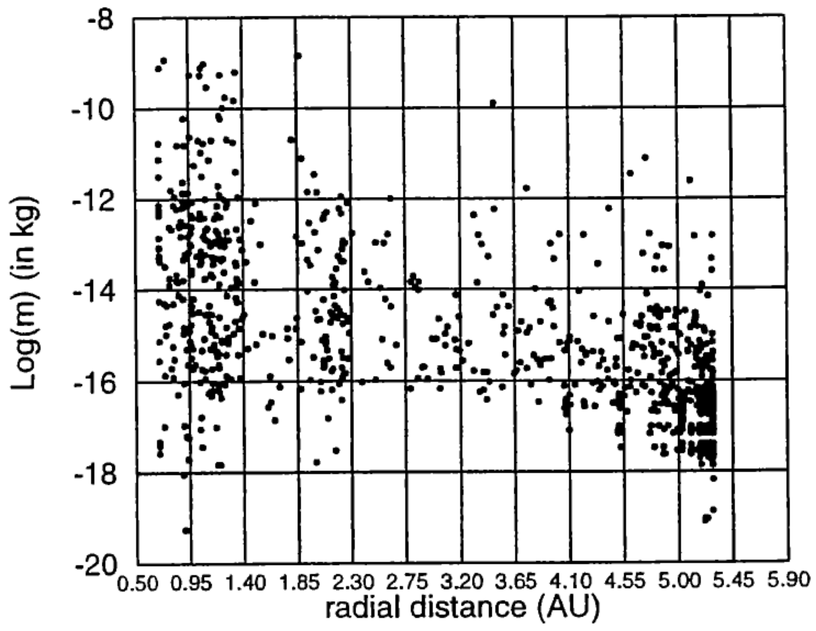

Fig. 3 Events in the (r_0, log m) plane showing statistics quality for each bin.

where m is the mass, r_0 is the radial distance in the ecliptic, $\mathbf{v}_{0e}$ is the in-ecliptic velocity vector and v_{0z} the out-of-ecliptic velocity component. Both standard deviations σ_e and σ_z, and both average in-ecliptic velocity vector $\mathbf{U}_e$ and out-of-ecliptic velocity component U_z are supposed to be function of r_0 and m. In order to account for the density decreasing with the radial distance we include a power law $r_0^{-\nu}$ (ν>0)

3.4 Choice of gaussian parameters functions of (r_0 ,m)

The choice of these functions is based upon a statistical study of the impacts on Galileo and Ulysses, the meteor radiants[14] data set and upon considerations on dust dynamics. We have distributed the events shown on Fig.3 into 6 mass bins ranging from 10^{-20} to 10^{-8} kg, and 12 radial distance bins ranging from 0.5AU to 5.9AU. In each cell we computed the average velocity components and the associated standard deviations of the processed data. Fig. 2 represents the average azimuthal component and its relative position with respect to the circular orbital velocity at the same distance. The quality of statistics in a given bin is directly linked to the time spent by the probe in that bin. Galileo flew once by Venus and twice by the Earth. This improves a lot the statistics quality between 0.7 AU and 2 AU where a lot of impacts have been detected.

Statitics show an average out-of-ecliptic velocity component very close to 0 for each range of mass which confirms assumption $\mathbf{H_2}$. Therefore in this representation, U_z is set to zero.

3.4.1 Radial velocity

The radial velocity is strongly biased. In its orbital motion, Galileo preferentially detects particles which orbit the Sun with a slightly positive radial velocity if Galileo moves towards the Sun and slightly negative if Galileo moves away from the Sun (the most probable direction is about 60 deg. inclined on the positive spin axis[2]). The same phenomenon appears for Ulysses, but this time it prefers positive radial velocity as it remains only in the ecliptic during its journey to Jupiter and because the most probable direction is 95 deg inclined on the positive spin axis[3]. On a closed orbit, two orbital positions exist with the same radial distance. They have opposite radial velocity components which are both taken into account in our formalism ($\mathbf{H_1}$). Thus, the average is zero. The Poynting-Robertson effect spirals intermediate-sized (10^{-14} to 10^{-8} kg) particles towards the Sun reducing eccentricity towards 0. This urges to assume a zero average radial velocity for every kind of particles.

3.4.2 Azimuthal velocity

Particles with m>10^{-8} kg are mainly on low eccentric orbits so that their average azimuthal velocity is very close to the keplerian one (Fig. 2). Beyond 2 AU the average velocity is much lower than the local keplerian one because particles are generally near their aphelion where the velocity is smaller. This velocity may tend towards zero for hyperbolic orbits of some very small particles (m<10^{-14} kg). The average azimuthal velocity detected at 1 AU for prograde orbits is 29.7 km/s which is in good agreement with our interpretation. Thanks to statistically relevant points picked up from Fig.3, we choose to reproduce the observed shape with the following parametric representation

$$U_t = \delta \frac{U_0}{r_0^{\alpha}} \frac{0.66 + e^{\beta u + \gamma}}{1 + e^{\beta u + \gamma}}, \qquad (7)$$

which involves four free parameters $\alpha,\beta,\gamma,\delta$ and the mass logarithm u.

3.4.3 In-ecliptic standard deviation

Near 1 AU, the statistics from 10^{-8} to 10^{-18} kg is good (Fig. 3) and the computed standard deviations obtained are quite reliable. The in-ecliptic observed standard deviation, obtained from radar meteors radiants, is about 15 km/s. At this distance, the standard deviation decreases with decreasing mass before reaching a minimum. Then it increases again for very small particles. Life of large particles (m>10^{-8} kg) is dominated by collisions which give to this population a natural dispersion. The Poynting-Robertson effect narrows the velocity distribution for smaller particles (10^{-14} to 10^{-8} kg) until the high number of collisions due

to high density of very small particles ($m<10^{-14}$ kg) increases again.
As we have very little information on particles with $m>10^{-8}$ kg except in the vicinity of 1AU, we will consider that their dispersion in the ecliptic is almost constant with the radial distance. Collisions increase the dispersion at low heliocentric radial distances. In order to account for these tendencies and to keep this shape when tuning parameters are varying, we decided to take this two-fold representation

$$\begin{cases} u \le \bar{u}: \sigma_e = \left(\sigma_m^1 - \Delta\sigma_1 e^{-\frac{(u-\bar{u})^2}{25}} \right) e^{-\frac{\alpha}{2}\left(1-\tanh\left(\frac{u-\bar{u}}{\beta}\right)\right) r} \\ u \ge \bar{u}: \sigma_e = \left(\sigma_m^2 - \Delta\sigma_2 e^{-\frac{(u-\bar{u})^2}{18}} \right) e^{-\frac{\alpha}{2}\left(1-\tanh\left(\frac{u-\bar{u}}{\beta}\right)\right) r} \end{cases} \quad (8)$$

where, σ_m^1, σ_m^2, $\Delta\sigma_1$, $\Delta\sigma_2$, $\bar{u}$, β and α are free parameters.

3.5 Out-of-ecliptic standard deviation

At 1 AU we observe a similar smoother valley-shape variation with respect to mass. Very small particles ($m<10^{-14}$ kg) are dispersed by the electromagnetic effects. Leinert et al.[12] suggest that the spread in orbital inclination around ecliptic follows a law proportional to $r^{1/2}$. As the out-of-ecliptic velocity component at both ascending and descending nodes is directly linked to $\sin i$, we will take the same kind of law for the velocity standard deviation. The standard deviation at large heliocentric distances is near zero and increases near the Sun because of collisions. For particles with $m>10^{-8}$ kg the standard deviation is almost constant. At 1AU the statistics on radar meteors give about 20 km/s. We took the following representation for the standard deviation.

$$\sigma_z = \frac{\sigma_0 \exp\left(-re^{-\frac{(u-\bar{u}')^2}{2\sigma^2}}\right)}{1+4\exp\left(e^{-\frac{(u-\bar{u}')^2}{2\sigma^2}}\right)} \; r^{0.5\left(1+\tanh\frac{u-\bar{u}'}{\beta}\right)}, \quad (9)$$

where σ_0, $\bar{u}'$, σ and β' are free parameters.

4. OPTIMIZATION OF THE REPRESENTATION AND DETERMINATION OF THE MODEL

The parametric representation described with equations Eq.6, Eq.7, Eq.8, and Eq.9 is constrained by the available measurements using a conjugate gradient algorithm which searches for the local minimum. The function to be minimized represents the RMS error made by the model while trying to reproduce the measurements. As we must assess such diverse physical quantities as zodiacal light, impact flux, impact rate, impacts, and velocity distributions, we use a common way of writing the error between model assessment val_{mod} and actual measurement val_{meas}. The RMS error[1] is incremented as follows

$$RMS = RMS + \left[\log\left|\frac{val_{mod}}{val_{meas}}\right| \Big/ \left(1 - \log\left|\frac{val_{mod}}{val_{meas}}\right|\right)\right]^2 . \quad (10)$$

If $val_{mod}=val_{meas}$ then the increment is zero. If $val_{mod}>>val_{meas}$ or $val_{mod}<<val_{meas}$ the increment is 1. We will now explain how we compute val_{mod} for the different kinds of observation.

4.1 Flux, impact rate, impacts, distribution functions

As probes orbit the Sun at very low inclination (except Ulysses), we will consider that instruments which perform impact detection remain in the ecliptic plane. The expression of the number of particles which impact the detector during a time interval Δt makes use of the sensor average detection area[2,3] S, the detection threshold[2,3] Th (function of impact velocity magnitude and mass which is 1 if the impact is detected and 0 if not), and the mathematical representation defined in paragraph 3. One can write

$$\Delta N = \Delta t \frac{1}{r_0^{\nu}} h(u) 10^u \ln 10 \, du \, Th\left(\left|\vec{\mathbf{w}}_i + \vec{\mathbf{U}} - \vec{\mathbf{V}}_{sp}\right|, u\right) \cdots$$
$$\cdots S(\gamma_i)\left|\vec{\mathbf{w}}_i + \vec{\mathbf{U}} - \vec{\mathbf{V}}_{sp}\right| e^{-\frac{\vec{\mathbf{w}}_\perp^2}{2\sigma_e^2}} e^{-\frac{w_z^2}{2\sigma_e^2}} dw_z w_\perp dw_\perp d\alpha \quad (11)$$

where $u=\log m$, $\mathbf{w}_i$ is the thermal velocity with its component vector $\mathbf{w}_\perp=(w_\perp,\alpha)$ perpendicular to the spin axis and its component w_z along it, $\mathbf{U}$, σ_e and σ_z are the average velocity vector the in-ecliptic and out-of-ecliptic standard deviations for mass m and radial distance r_0. A Monte-Carlo sampling is performed to evaluate the total number of impacts received during the time step Δt. We convert the information of each sample into impact rate, flux and velocity distribution. For radar meteors, the detecting surface is modeled by a flat plate whose average sensing area is a cosine function of the angle from the radar axis.

4.2 Zodiacal light

The calculation of zodiacal light is based upon the scattering partition function $B(\theta)$ of the particle which is derived from Leinert et al.[12] and the cross-section partition function[7] $A(u)$. The zodiacal light observed at distance R_{obs} along the line of sight (β,ε) (Fig.4) is reproduced by our model as follows

$$I = \frac{F_0 R_0^2}{R \sin\gamma} \int_\gamma^\pi dB(\theta) \int_{-\infty}^{+\infty} dA(u) \int_{R_{\min}}^{R_{\max}} dr_0 \cdots$$
$$\cdots \int_{-\infty}^{+\infty} d\,erf\left(\frac{v_{t0}}{\sigma_e\sqrt{2}}\right) \int_{-\infty}^{+\infty} d\,erf\left(\frac{v_{z0}}{\sigma_z\sqrt{2}}\right) \cdots \quad (12)$$
$$\cdots \frac{1}{r_0^{\nu}\sigma_e} \exp\left[-\frac{\left[v_r - U_r\right]^2}{2\sigma_z^2}\right] J\left(v_{t0}, v_{z0}, r_0\right) \left|\vec{\mathbf{v}}\right| \Big/ \left|\vec{\mathbf{v}}_0\right| ,$$

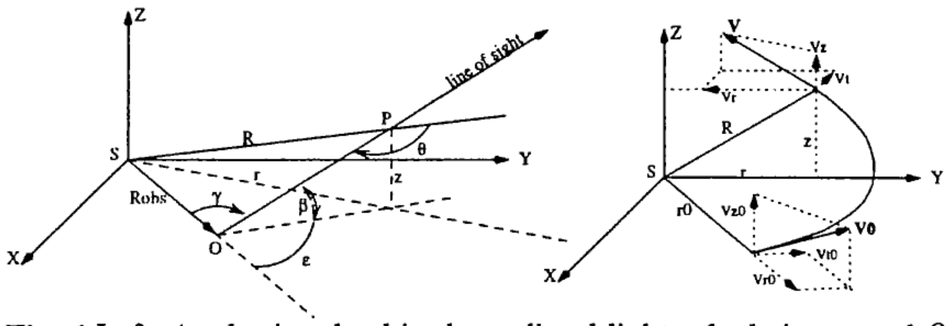

Fig. 4 Left: Angles involved in the zodiacal light calculation. ε and β characterize the line of sight and R_{obs} the detector position. Right: connection between in- ecliptic and out-of-ecliptic position.

where standard deviations σ_e and σ_z are function of u and r_0, U_r is a function of v_{t0} and v_{z0} and J is the Jacobean of the $(v_{r0}, v_{t0}, v_{z0}) \rightarrow (r_0, v_{t0}, v_{z0})$ transformation. For each scattering point and a given velocity $\mathbf{v}$ at this point a unique ascending velocity $\mathbf{v}_0$ is defined in the ecliptic. Instead of using $\mathbf{v}_0$ components as integration variables we prefer (r_0, v_{t0}, v_{z0}) which are more convenient for Monte-Carlo sampling.

4.3 Results

The model gives velocity distributions that are in pretty good agreement with the processed data (Fig. 5). The peaks and their intensities are respected before 2.5 AU. Beyond this limit the peak intensity and position are different from to the processed data one. The zodiacal light is not fitting very well the experimental data when the observer is close to the Sun (Helios I trajectory[11]) and when the line of sight points in a direction close to the Sun ($\varepsilon \approx 40$ deg.). The model gives a flux impact rate on Pioneer 10&11 close to the measurement before 4AU. Beyond this limit the model seems to underestimate the measurements. A beginning of explanation is the absence of interstellar particle flux model.

The flux computed along the Galileo trajectory is in good agreement with data and Divine's model[1] (Fig. 6). The curve obtained during the Ulysses ecliptic traverse (Fig. 7) from our model, clearly shows a lack of particles in the out-of-ecliptic medium, and a little overestimation in the ecliptic vicinity. The model does not account for interstellar particles which are dominant at high latitudes[9]. That explains the differences. The overestimation is not yet explained.

As a summary, the model does not fit very well out-of-ecliptic fluxes, measurements made close to the Sun and at large heliocentric distances.

5. DISCUSSION

This mathematical representation allows an analytical mapping of the adiabatic invariants phase space $(\mathcal{E}, \mathcal{G}, \mathcal{H}, \omega)$ by means of equation Eq.6 and the following transformation formulae from one space to the other

$$v_{0r} = \frac{\mu}{\mathcal{G}} \sin\omega \sqrt{1 + \frac{2\mathcal{E}\mathcal{G}^2}{\mu^2}},$$

$$v_{0t} = \frac{\mu}{\mathcal{G}} \left(1 + \sqrt{1 + \frac{2\mathcal{E}\mathcal{G}^2}{\mu^2}} \cos\omega \right) \frac{\mathcal{H}}{\mathcal{G}}, \qquad (13)$$

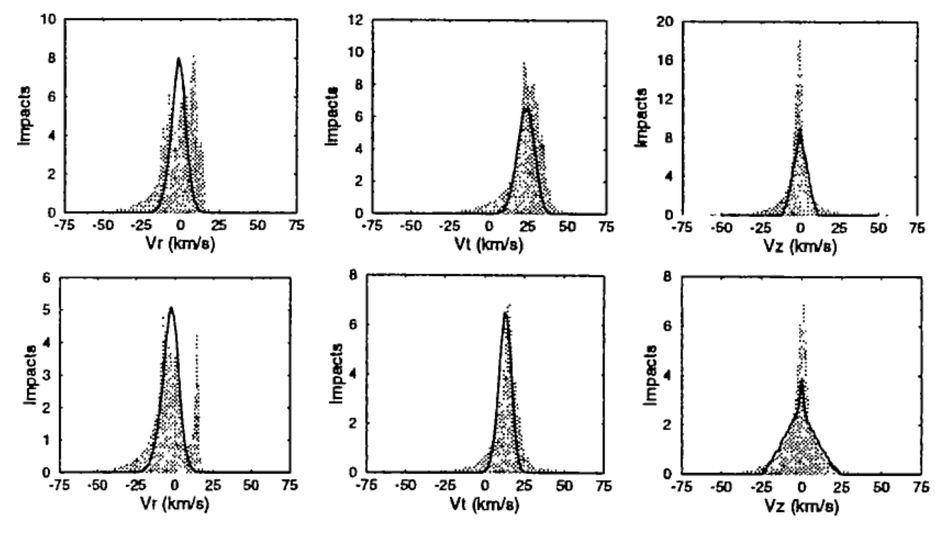

Fig. 5 Comparison between model (solid line) and Monte-Carlo processed Galileo data (shaded curve). From left to right radial, azimuthal and out-of-ecliptic velocity components are displayed. The upper line represents the distance 1.175 AU and the lower one 2.075 AU

$$v_{0z} = \frac{\mu}{\mathcal{G}} \left(1 + \sqrt{1 + \frac{2\mathcal{E}\mathcal{G}^2}{\mu^2}} \cos\omega \right) \sqrt{1 - \frac{\mathcal{H}^2}{\mathcal{G}^2}}.$$

$$r_0 = \frac{\mathcal{G}^2/\mu}{1 + \sqrt{1 + \frac{2\mathcal{E}\mathcal{G}^2}{\mu^2}} \cos\omega}$$

This mathematical representation involves μ which is the gravitational constant associated to the Sun gravitation. For particles with mass between 10^{-14} and 10^{-20} kg the effect of the solar pressure cannot be neglected.

Some particles may experience injections on repulsive hyperbolic orbits if solar radiation is too strong ($\beta > 1$)*. The model presented here is not yet able to include such trajectories and cannot represent these particles. A systematic cut-off is implemented at 10^{-17} kg where $\beta \approx 1$. Moreover, in this description β-meteoroids which are produced in the vicinity of the Sun and ejected from solar system on hyperbolic orbits have size beyond Ulysses and Galileo detector threshold[2,3]. The model for particles under 10^{-14} kg is still uncertain.

It is possible with this formulation to compute macroscopic quantities of the cloud simply using the relation between two positions on the same orbit. The out-of ecliptic mapping is the following (using $\mathbf{H_3}$)

$$f(r, z, \vec{\mathbf{v}}) = f(r_0, \vec{v}_0) \frac{|\vec{\mathbf{v}}_0|}{|\vec{\mathbf{v}}|} \qquad (14)$$

where r_0 and v_0 are function of r, z, and $\mathbf{v}$. (r, z, $\mathbf{v}$) are calculated through the successive transformations (r, z, $\mathbf{v}$)$\rightarrow$($\mathcal{E}, \mathcal{G}, \mathcal{H}, \omega$) $\rightarrow$(r_0, $\mathbf{v}_0$.). Macroscopic quantities may be derived from Eq.14 as follows

$$P = \iiint p(\vec{\mathbf{v}}) \frac{|\vec{\mathbf{v}}_0|}{|\vec{\mathbf{v}}|} f(r_0, \vec{v}_0) \left| \frac{\partial \vec{\mathbf{v}}}{\partial \vec{\mathbf{v}}_0} \right| d\vec{\mathbf{v}}_0. \qquad (15)$$

If the function p is equal to 1, $\vec{\mathbf{v}}$ and v^2 the macroscopic quantity P is density, average velocity and energy.

---

* β is the ratio of the radiation pressure to the gravity magnitude.

6. CONCLUSION

From Ulysses and Galileo directional information and dust dynamics considerations we derived a new mathematical model of the dust cloud, different from the one used by Divine.
Its results in the ecliptic are in good agreement with measurements between 0.5 and 3 AU but is uncertain for particles whose mass is lower than 10^{-14} kg. β-meteoroids and interstellar particles are to be modeled separately in order to span the mass range from 10^{-21} to 10^{-14} kg and enhance the model accuracy.
It yields analytical out-of-ecliptic and adiabatic invariants phase space mappings and macroscopic quantities evaluation. Its gaussian shape is convenient for Monte-Carlo computation techniques and the link with adiabatic invariants is convenient for long time scale numerical simulations such as secular evolution.

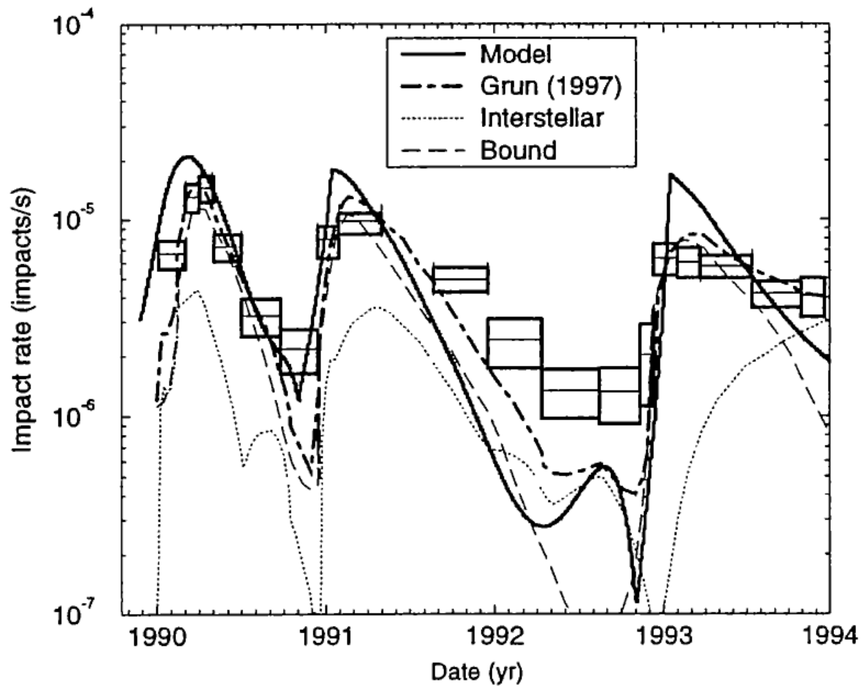

Fig. 6 Impact rate experienced by Galileo from 1990 to 1994. Comparison between our model (solid line), modified Divine model[8](Grün et al. 1997 - dotted dashed) and measurements (boxes). Interstellar population and bound population added by Grün et al. to the old Divine's model[1] are displayed.

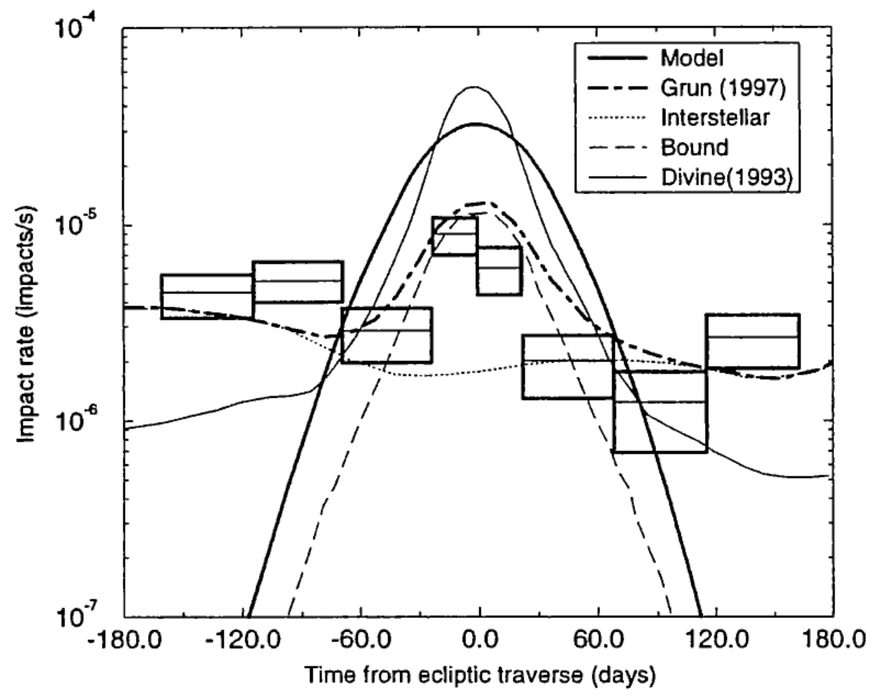

Fig. 7 Impact rate experienced by Ulysses during its first ecliptic traverse. Comparison between our model (thick solid line), modified Divine's model[8](Grün et al. 1997 - dotted dashed), old Divine's model[1] (1992 - thin solid line) and measurements Interstellar and bound populations added by Grün et al. to the old Divine's model are displayed

7. REFERENCES

1. Divine N., Five populations of Interplanetary meteoroids, in *Journal of Geophysical Research,* 98, pp 17029-17048, Sept. 1993.

2. Grün E., The Galileo dust detector, *Space science review*, 60, pp 317-340, 1992.

3. Grün E., The Ulysses dust experiment, *Astronomy and Astrophysics Supplement Series*, 92, pp 411-423, January 1992.

4. Grün E., Three years of Galileo Dust Data, *Max Planck Institut für Kernphysik, Heidelberg*, 1994.

5. Grün E., Two years of Ulysses Dust Data, *Max Planck Institut für Kernphysik, Heidelberg*, 1994.

6. Grün E. et al., Interstellar dust in the heliosphere, *Astronomy and Astrophysics*, February 1994.

7. Grün E. et al., Collisional balance of the meteoritic complex, *Icarus*, 62, pp 274-272, 1985.

8. Grün E., Staubach P. et al., South-North and Radial Traverses Through the Interplanetary Dust Cloud, *(To be published in Icarus)*, 1997

9. Grün E., Zook H. A.. et al., Discovery of jovian dust streams and interstellar grains by the Ulysses spacecraft, *Nature*, 362, pp 428-430, 1993

10. Leinert C. et al., Results of Pioneer 10 and 11 meteoroid experiments: Interplanetary and near-Saturn, in *Journal of Geophysical Research*, 85, pp 5841-5852, November 1980.

11. Leinert C. et al., The zodiacal light from 1.0 to 0.3 A.U. as observed by the Helios Space Probes, in *Astronomy and astrophysics*, 103, pp 177-188, 1981.

12. Leinert C. et Grün E., Interplanetary Dust, in *Physics of the inner heliosphere N°1*, pp 207-275, Springer Verlag, 1990.

13. Levasseur-Regourd A.C. et Dumont R., Absolute photometry of zodiacal light, *Astronomy and Astrophysics*, 84, pp 277-279, June 1980.

14. Lindblad L.A., The IAU meteor Data Center in Lünd, *A.C. Levasseur-Regourd and H. Hasegawa Editions, Origin and Evolution of Interplanetary Dust*, pp 311-314, 1991.